Variable Voltage Bus Concept for Aircraft Electrical Power System

Seang Shen Yeoh, Mohamed Rashed, *Member, IEEE*, Mike Sanders, and Serhiy Bozhko, *Senior Member, IEEE*

***Abstract*— The paper deals with the innovative concept of "variable voltage" bus concept for future more-electric aircraft platforms. Using new functionalities and opportunities offered by innovative sources actively controlled by power electronics, there is an opportunity for significant increase of their output power (within powertrain capabilities, machine thermal limits and power converter maximum current) to supply increased load demands under certain conditions. The paper investigates application of this concept to satisfy power demands for wing ice-protection system for business-jet. The study includes detailed study into the control challenges of the proposed approach and suggests corresponding theoretical solutions. Furthermore, the controller design aspects are explored with considerations to achieve stable operation. The concept is tested in simulation environment and validated through experimental studies. This paper might be of interest for the researchers and engineers focused on innovative solutions for future aircraft platforms.**

***Index Terms*— control design, icing protection system, more electric aircraft, variable voltage control, voltage wild**

I. INTRODUCTION

The design of next-generation aircraft platforms has been targeting for more efficient and hence more environmentally friendly, greener solutions to ensure sustainable future. In more-electric aircraft (MEA), this is achieved by replacement of on-board systems powered by hydraulic and pneumatic energies by electrically powered ones [1-3]. Because of this transfer, the total installed on-board electrical power demand in future aircraft will significantly increase. One of these "new" loads on-board MEA is the wing ice-protection system (WIPS) which employs electrically produced heating using resistive thermal mats. In larger aircraft this load system can typically demand about 125kW per wing [4] and this is within the available poser budget. Conversely, for smaller platforms such as regional and business airplanes, the total generated on-board power may not be enough to cover the WIPS demand. Therefore, hybrid solutions are considered where these assumes employment of bleed air from the engine in combination with the electro-thermal mats. Some other new/existing designs consider electro-expulsion or electro-mechanical methods of removing formed ice [5], [6] which requires the least amount of energy but are not very reliable and may lead to the wing structural damages. Others have chemical de-icing systems [5], which are of limited availability during a flight cycle, and piezo-electric based technologies that has drawbacks in electromagnetic interference and wing structural fatigue [5].

In current fully electrical WIPS solutions (eWIPS) the electric power distribution is arranged via the main buses of an aircraft electrical power system (EPS) [7-9]. As illustrated in Fig. 1(a), the eWIPS is connected to a fixed high voltage bus along with other electrical loads. Local power converters/controllers can be used to vary the amount of power to the eWIPS depending on the temperature requirement and zonal heating capabilities [10]. One thing to note is that both ac and dc power transmissions are viable as the eWIPS is mainly resistive in nature. For the topology of this EPS, the voltage levels should be kept constant as the bus may be shared with other more sensitive electrical loads. Hence, the bus voltage level and total resistance of the thermal mats limit the maximum eWIPS power.

There are possible control methods of transmitting power from the power source to the eWIPS if the primary sources are based on innovative topologies such as permanent magnet machine (PMM) controlled by active front-end power electronic converter [3, 11]. In literature, [12] has described a vector based control scheme including its controller design steps for PMM based aircraft starter-generator systems. [13] proposed a control scheme based on voltage angle regulation for high speed PMM based drive systems. The control scheme allows full utilisation of the dc bus voltage and improved control stability using d-axis feedback loop. A similar control concept was also presented in [14] based on voltage angle with six step operation and the inclusion of d-axis current loop for added controller stability. De-centralised droop based control strategy for paralleled multi-generator system for MEA has been looked at in [15] and [16].

If the bus voltage level is not restricted, there is a natural opportunity to increase its output voltage by narrowing the region of flux-weakening operation within the current limits of power converter and torque capabilities of the power train

Manuscript received June 30, 2018; revised August 28, 2018 and October 21, 2018; Accepted November 2, 2018. This project has received funding from the Clean Sky 2 Joint Undertaking under the European Union's Horizon 2020 research and innovation programme under grant agreement No CS2-AIR-GAM-2014-2015-O1. Cf. Art.29.4 of [A2].

Mike Sanders is with Meggitt Polymers & Composites, Shepshed, LE12 9EQ, U.K. (e-mail: Michael.Sanders@meggitt.com)

The other authors are with the Department of Electrical and Electronic Engineering, University of Nottingham, Nottingham NG7 2RD, U.K. (e-mail: Seang.Yeoh@nottingham.ac.uk; Mohamed.Rashed@nottingham.ac.uk; Serhiy.Bozhko@nottingham.ac.uk).

(accessories gearbox). Within the current limit, this would mean that there is reduced reactive current component and hence increased allowance for active part while not affecting the machine thermal performance. This can be achieved via a dedicated bus for the eWIPS as seen in Fig. 1(b). When the eWIPS demands for very high power level, e.g., if anti-icing required, then "above the rated" voltage levels can be set and this can be called variable voltage, or "voltage wild" bus. Furthermore, such configuration eliminates the need for local eWIPS power converters and may yield potential reduction in overall aircraft weight.

The drawback for this concept is that the increase in bus voltage also increases the semiconductor losses assuming same current operation levels and the need for appropriate circuit protection devices. Hence, the converter, cooling system, and circuit protection devices may have to be over-rated to compensate for the losses. Moreover, the voltage variation should be within the maximum limits of the electrical machine as partial discharges may occur.

This paper investigates the theoretical aspects of "voltage wild" EPS concept, including overall control approach, controllers design and stability analysis. The key theoretical findings are supported by the EPS simulations at different operational modes and verified by a mock-up EPS. Details of the studied EPS is in Section II and its proposed control scheme in Section III. In-depth controller design and analysis are reported in Section IV, followed by both simulation and experimental results in Section V and VI respectively. Section VII concludes the paper.

II. Power System

The base EPS explored for this study is illustrated in Fig. 2. ω_r is the mechanical speed, i_{abc} is the three phase stator current, C is the dc bus capacitance, and R_w is the eWIPS load. Here, the generator is assumed to be connected only to the eWIPS as to determine and test a suitable control scheme. The high-level control scheme covering the interactions between multiple buses is not covered in this paper. A generator system considered for this study consists of a PMM that can be mechanically coupled to the aircraft engine.

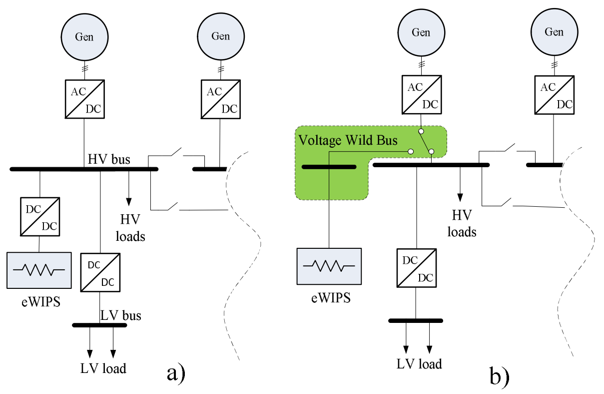

Fig. 1. (a) eWIPS integration in current MEA EPS architectures and (b) the proposed integration.

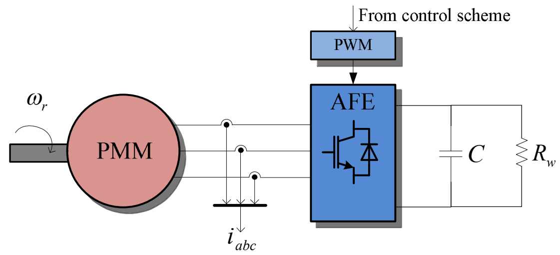

Fig. 2. MEA EPS in investigation.

An active front end rectifier (AFE) is connected to the PMM which converts ac power generated by the PMM to dc power and transfers to the bus. The AFE can be controlled via pulse width modulation (PWM) generated from the control scheme signals. A resistor is used to represent the eWIPS that is assumed fully resistive in nature.

The key equations representing the system can be seen from (1) to (4). They are denoted in the widely used rotating reference dq frame for three phase drive systems [17]. v_d, v_q, i_d, and i_q are the ac voltages and currents in dq frame. R_s, L_d, L_q, and ψ_m are the PMM stator resistance, inductances, and machine flux respectively. i_{dc} and E_{dc} are the dc current and voltage while ω_e is the electrical speed.

$$v_d = R_s i_d + L_d \frac{di_d}{dt} - L_q \omega_e i_q \tag{1}$$

$$v_q = R_s i_q + L_q \frac{di_q}{dt} + \omega_e (L_d i_d + \psi_m) \tag{2}$$

$$E_{dc} i_{dc} = -\frac{3}{2}(v_d i_d + v_q i_q) \tag{3}$$

$$C\frac{dE_{dc}}{dt} = i_{dc} - \frac{E_{dc}}{R_w} \tag{4}$$

III. Control Scheme

Typically, the control priority for an aircraft generator system is the bus voltage for nominal load operation and current limit regulation within the EPS rating. In [12], speed control was selected for starter operation while bus voltage control with droop coefficients was used in generation mode. For both modes, flux weakening control is always present in the event of operation at high speeds to preserve power converter controllability. Similar control scheme was introduced in [15] with the use of droop based bus voltage controller focusing on its design and stability analysis. Classic bus voltage control was used in [18], [19] and [20]. Their control schemes seemed sufficient for the priorities mentioned earlier, however an alternative control scheme has to be considered to introduce the "voltage wild" concept. An additional function to control is the power of the eWIPS load that will vary the bus voltage levels.

As such, there are four different functions that have to be performed by the control scheme:

1) Flux weakening for the PMM during high speed operation.
2) Keeping E_{dc} constant when connected to the normal bus.
3) Regulate eWIPS power when connected to the eWIPS bus.
4) Regulate stator current within the designated limit.

The proposed control scheme will facilitate all four functions in order to enable the variable voltage concept. The functionalities allow constant/variable bus voltage control depending on the bus it is connected to. Flux weakening is employed when needed to maintain converter controllability and in addition to that, stator current limit controller. The control structure would then be able to prioritise these functions depending on the operating modes (speed and load) and reference values.

The control structure for this study is shown in Fig. 3. The structure can be divided into two parts; the inner and outer loops. The inner loop consists of the *dq* current controllers (W_{id} and W_{iq}) and a dynamic modulation index limit. m_{abc}, m_d, and m_q are the modulation index in three phase and *dq* frame respectively. $m_{\lim}$ is the maximum modulation index and $m_{d\lim}$ is the limit imposed on m_d. The value of k_s depends on the modulation scheme to be used for the power converter [21]. The outer loop is made up of dc voltage, current limit, and dc power controllers (W_e, W_{is}, W_p) with back-tracing (BT) algorithm. i_{q1}^*, i_{q2}^*, and i_{q3}^* correspond to the outer loop controllers output respectively. i_s and i_{smax} are the stator current and its maximum value, while P_{dc} is the dc power. Variables with the * superscript denotes its corresponding reference signal. This control scheme covers the four functions listed previously with the dynamic limit to maintain converter controllability and the remaining outer control loops for their respective functions.

A. Inner control loops

The operating principal for the dynamic limit is based on the following equation:

$$m_{\lim} \geq \sqrt{m_d^{\,2} - m_q^{\,2}} \tag{5}$$

The modulation index is the ratio between the AC voltages to E_{dc} through:

$$m_d = \frac{v_d^{\,*}}{E_{dc}k_s}, m_q = \frac{v_q^{\,*}}{E_{dc}k_s} \tag{6}$$

For this study, $m_{\lim}$ is set to 1 for full utilisation of the available voltage supplied by the PMM. The q-axis control loop should have higher priority than d-axis, hence m_d can be limited to fulfil the conditions of (5):

$$m_{d\lim} = \sqrt{m_{\lim}^{\,2} - m_q^{\,2}} \tag{7}$$

Flux weakening is achievable through this modulation index limit (5), where $m_{d\lim}$ dictates the output m_d which determines the amount of reactive current represented by i_d into the PMM to reduce the back-emf. The current loops are set to control the stator currents in *dq* frame. W_{id} has a fixed reference value of zero. This will ensure that i_d is controlled to be zero when the modulation index is less than its limit. On the other hand, i_q^* is dictated by the outer loop controllers and determines the value of m_q and $m_{d\lim}$. The output of the current controllers are scaled by $E_{dc}k_s$ to obtain the respective modulation indexes using (6).

B. Outer control loops

The function of W_e is to maintain constant E_{dc} (typically 270V for high voltage dc buses) in the event that the EPS is connected to a normal bus. It can also be used with the eWIPS bus if only nominal power is required. W_{is} serves as a current limit to address the disadvantage of this type of control structure. The output of W_{is} (i_{q2}^*) is multiplied by the sign of i_q^* to ensure correct power flow direction. When i_s exceeds the reference value, i_{q2}^* reduces in order to meet the requirements of:

$$i_{s\max} \geq \sqrt{i_d^{\,2} + i_q^{\,2}} \tag{8}$$

If i_s is less than i_{smax}, then W_{is} output is limited to zero to prevent control conflict with the other outer loop controllers.

The third outer loop controller is W_p that regulates the power required for the eWIPS load. This controller is setup for uni-directional power flow to only send power to the dc bus. The control idea is straightforward, which is to control the power sent to the eWIPS load. The power demand should be derived from the temperature requirement of the eWIPS load with respect to the surrounding temperature. However, in this paper it is assumed that the power demand is determined by the user in order to simplify the control design process. This controller becomes a priority when the power demand exceeds the power supplied using W_e (P_{dc} with given R_w at E_{dc}^*). In general, the magnitude of error of the controllers determine the controller priority.

Each of the controllers can adopt the general PI configuration, utilising proportional and integral gains (k_p and k_i) to regulate the respective control variables. The controllers also use anti-windup scheme to prevent integrator saturation issues. The outputs of these controllers can be selected as reference values for i_q. A minimum function is used to compared all three signals and the smallest value is selected as i_q^*. The minimum value is used as the direction of current flow from the PMM towards the dc bus is considered to be negative. To ensure smooth transitions between the controller signals, BT algorithm is employed for all three controllers [22]. This algorithm takes into account the output i_q^* and maintains each controller integrator states to be of similar value. Fig. 4 shows a flow diagram that summarises in general the control action of the proposed control scheme.

IV. Control Plant

In this Section, the control plants are defined to aid the control design process. It can be observed that there are non-linearities in the equations of the EPS such as (3), (5), and (6). They are linearised using Taylor's approximation around a particular operating point for small signal analysis. An assumption made is that ω_e is constant for small signal analysis as the speed changes are much slower than the electrical variables. The following are the small signal equations to be used to derive the outer control loop plants, and the corresponding small signal variables have the symbol

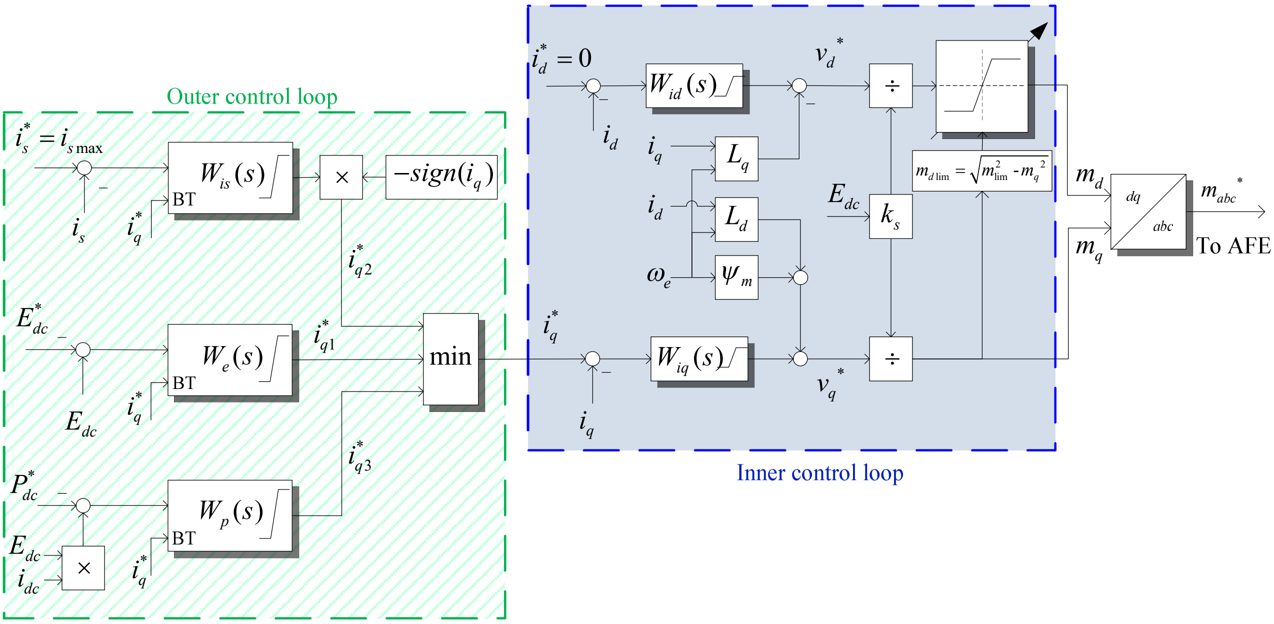

Fig. 3. Proposed variable bus voltage control scheme.

Δ. Any variable with the o subscript denotes its initial operating point value.

$$\Delta v_d = R_s \Delta i_d + L_d s \Delta i_d - L_q \omega_{eo} \Delta i_q \tag{9}$$

$$\Delta v_q = R_s \Delta i_q + L_q s \Delta i_q + L_d \omega_{eo} \Delta i_d \tag{10}$$

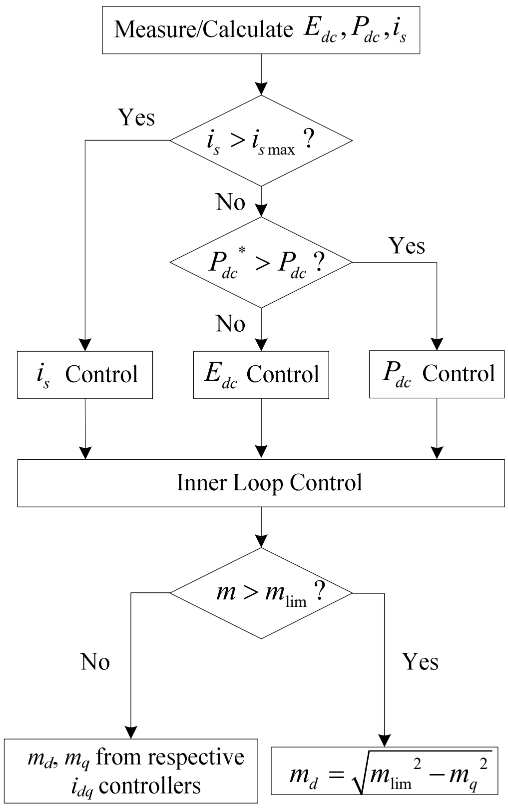

Fig. 4. Proposed control scheme flow diagram.

$$m_{do} \Delta m_d = -m_{qo} \Delta m_q \tag{11}$$

$$s \Delta E_{dc} = \frac{1}{C} \Delta i_{dc} - \frac{1}{R_w} \Delta E_{dc} \tag{12}$$

$$\Delta v_d = k_s m_{do} \Delta E_{dc} + k_s E_{dco} \Delta m_d \tag{13}$$

$$\Delta v_q = k_s m_{qo} \Delta E_{dc} + k_s E_{dco} \Delta m_q \tag{14}$$

A. Inner current control loop

The inner current loops design have been well established in literature [23]. One can form the closed loop plant for the current loops with PI type controller. For the i_q control loop:

$$\frac{\Delta i_q}{\Delta i_q^*} = \frac{k_{pq} s + k_{iq}}{L_q s^2 + (R_s + k_{pq}) s + k_{iq}} \tag{15}$$

The current controllers have been designed to achieve bandwidth of 400 Hz, damping factor ζ = 0.95 and the controller gains can be found in Appendix I.

B. DC voltage control loop

From (3), it can be seen that E_{dc} can be controlled through the variation of i_q (i_d is exclusive for flux weakening function) [21]. Therefore, the plant for this control loop can be developed starting from the linearised equation of (3):

$$\Delta i_{dc} = \begin{bmatrix} -\dfrac{3}{2E_{dco}} (v_{do} \Delta i_d + i_{do} \Delta v_d + v_{qo} \Delta i_q + i_{qo} \Delta v_q) \\ + \dfrac{3}{2E_{dco}^2} (v_{do} i_{do} + v_{qo} i_{qo}) \Delta E_{dc} \end{bmatrix} \tag{16}$$

Each small signal variable can be replaced with equations (9) to (15) such that an open loop plant relating single input i_q^* to single output E_{dc} can be established in (17). The coefficients for n_1, n_2, n_3, d_1, d_2, and d_3 are located in Appendix II.

$$\frac{\Delta E_{dc}}{\Delta i_q^*} = \frac{-3E_{dco}R_w(n_1 s^2 + n_2 s + n_3)}{(d_1 s^2 + d_2 s + d_3)} \frac{\Delta i_q}{\Delta i_q^*} \tag{17}$$

A comparison step response has been made between the derived transfer function with a non-linear model that consists of the equations (1) to (5). At a same operating point, both responses show good correlation and hence the transfer function can be considered as the plant for W_e.

The root locus at different loads were also plotted as depicted in Fig. 5. As the load power increases, there is a tendency for one of the poles to move towards the left side. A more important discovery is that there is a pair of conjugate zeroes that move closer to the imaginary axis as the load power increases.

If a pure integrator controller is used to form a closed loop transfer function, the trajectory of the closed loop poles can cross the imaginary axis to the left hand plane which causes instability. This can be seen in Fig. 6, and the controller should be designed carefully as there is a limited gain range that can guarantee stability. However, if a proportional term is added to the controller, then the root locus trajectory is confined within the right hand plane (RHP). This means that the controller is stable for all gain values and is selected for E_{dc} control.

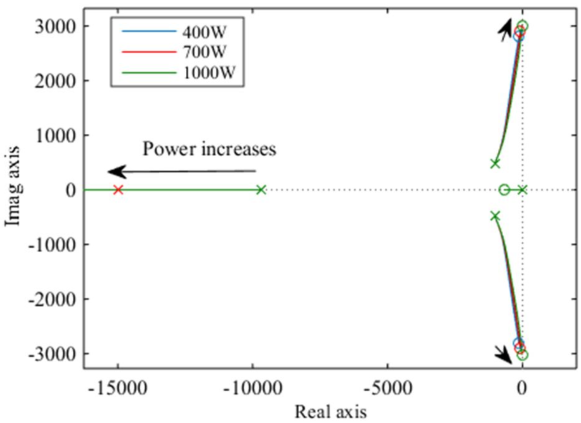

Fig. 5. E_{dc} open loop plant root locus at different load levels.

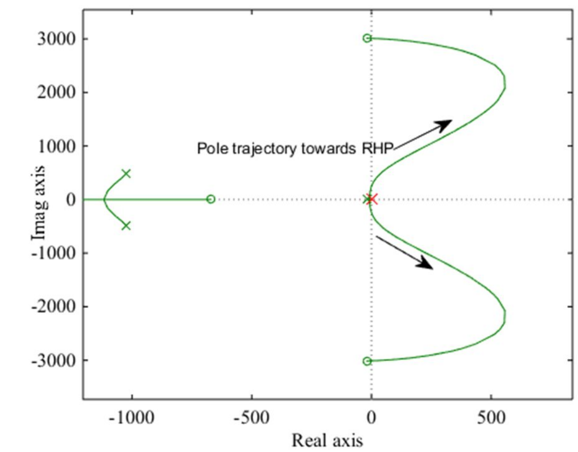

Fig. 6. Closed loop root locus for E_{dc} plant with I controller.

C. DC power control loop

The approach to derive the plant for P_{dc} control is similar to the E_{dc} plant, and can begin from the linearised equation for P_{dc}:

$$\Delta P_{dc} = i_{dco}\Delta E_{dc} + E_{dco}\Delta i_{dc} \tag{18}$$

Using the same set of equations, the plant can be derived as:

$$\frac{\Delta P_{dc}}{\Delta i_q^*} = (E_{dco}CR_w s + i_{dco}R_w + E_{dco}) \frac{\Delta E_{dc}}{\Delta i_q^*} \frac{\Delta i_q}{\Delta i_q^*} \tag{19}$$

The derived transfer function was also verified with an equivalent non-linear model. Since the open loop plant is closely related to the E_{dc} plant, it shares similar poles and zeroes location. Using an operating point when P_{dc} control is operational, the plant showed zeroes that are on the RHP as seen in Fig. 7. This shows non-minimum phase characteristics, and the controller will have a limited gain range that allows stable operation. Since the power fed to the load can be done by increasing E_{dc}, it is possible that m can be less than 1. As a result, the root locus has real positive zeroes instead as observed in Fig. 7. For the purpose of this study, it is assumed that the EPS always operates with m = 1, hence only the associated operating points are considered.

For the closed loop analysis, the gain limit for W_p is inversely related to the amount of power requested. The controller would have a small gain range for stable operation if the need for high power is required. Hence, it is recommended that small controller gains are selected for W_p. Fig. 8 shows the closed loop root locus for P_{dc} plant with PI type controller. The gain range was verified with an equivalent non-linear model where increased oscillations was observed when the controller gain exceeds the range. It can be seen that if proportional gains are used for the controller, its value has

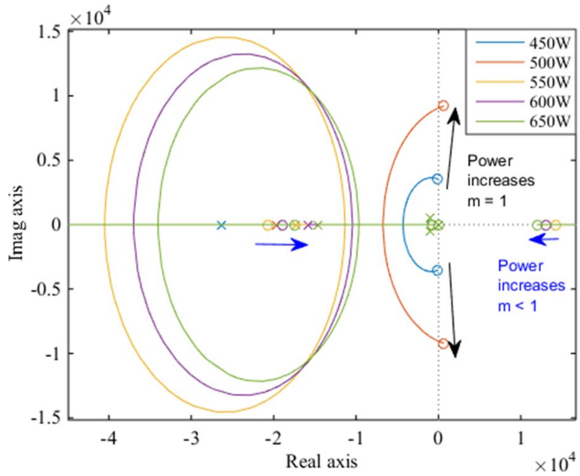

Fig. 7. P_{dc} open loop root locus at different power demand levels.

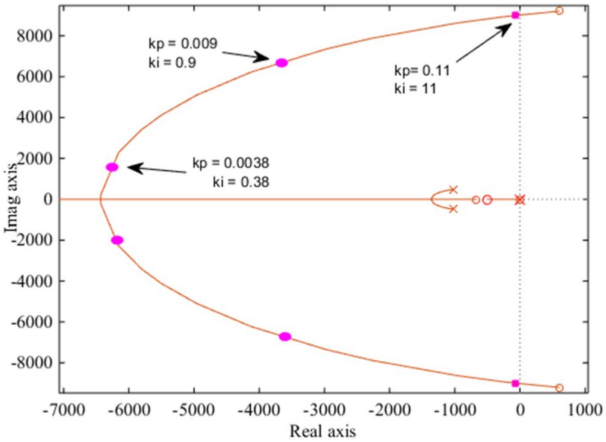

Fig. 8. Closed loop root locus for P_{dc} plant with PI controller.

to be small or instability may occur when the pole pairs (pink dots) cross to the RHP. Therefore, it is recommended to have an I controller instead where the controller gain has more stability range.

D. Current limit control loop

Since the stator current is the control variable for this loop, hence the plant can be derived from the linearised current limit equation (8):

$$\Delta i_s = \frac{i_{do}}{i_{so}} \Delta i_d + \frac{i_{qo}}{i_{so}} \Delta i_q \tag{20}$$

Similarly, using the equations (9) – (14), the plant for W_{is} can be found as shown in (21). The coefficients for n_4, n_5, n_6, d_4, d_5, and d_6 are located in Appendix II.

$$\frac{\Delta i_s}{\Delta i_q^*} = \frac{n_4 s^2 + n_5 s + n_6}{i_{so}(d_4 s^2 + d_5 s + d_6)} \frac{\Delta i_q}{\Delta i_q^*} \tag{21}$$

Fig. 9 shows the derived open loop plant root locus at different load points when the EPS is operating at current limit. This plant exhibits non-minimum phase characteristics as well, and the controllers would need to be designed carefully. The variation of load shows small changes to the positive zero locations that gradually moves to the real axis. Furthermore, there is a presence of a plant pole very close to the origin. This would mean that the controller bandwidth has to be slow (less than 10Hz), and the controller gain range can be very small. The use of I controller allows a slightly larger gain range, however at the cost of damping. The closed loop analysis using PI type controllers can be seen in Fig. 10. The addition of proportional term, allows more damping and also increased bandwidth allowance along the stable gain range. Hence, the PI type controller is selected to regulate i_s.

In summary, both P_{dc} and i_s plants have non-minimum phase characteristics and their controllers have limited stability gain range. The gain range can be determined through the derived plants at the desired load operating point. The

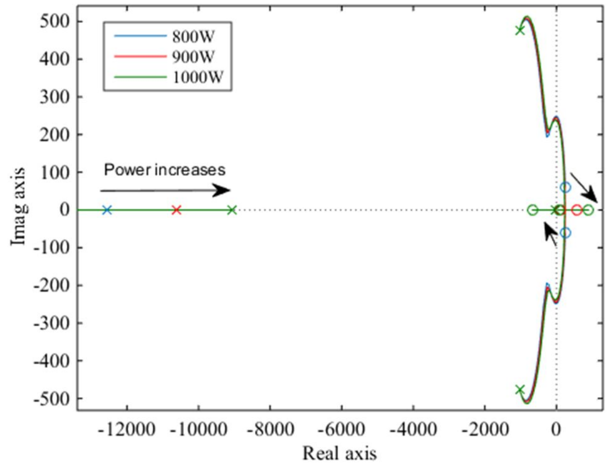

Fig. 9. i_s open loop root locus at different power demand levels.

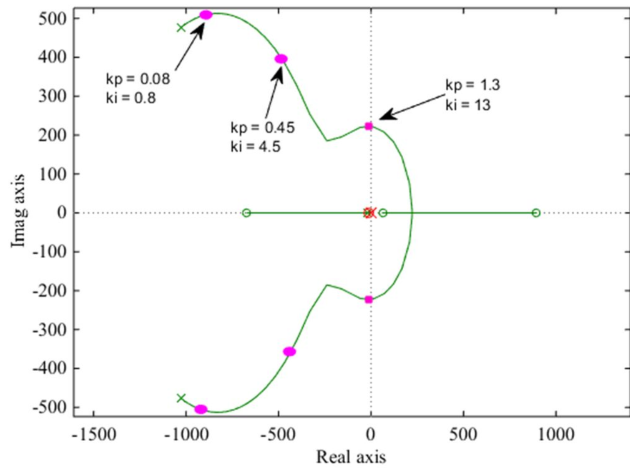

Fig. 10. Closed loop root locus of i_s plant with PI controller.

closed loop root locus of the derived plants can be used to select suitable gains for the respective controllers.

Taking into account the gain stability range (before having positive poles on the right half plane), the gain can be selected when the closed loop poles are ¾ distance away from the imaginary axis. This is to ensure stable operation of the controller while having reasonable dynamic response.

The following gains have been selected for the outer loop controllers to achieve reasonable bandwidth response within the stable ranges and they are displayed in Table I. The back-tracing gains have been selected as $k_{te} = k_{tp} = k_{ti} = 200$ that is much faster than the controller bandwidth to achieve fast tracking during controller transient changes.

TABLE I
OUTER LOOP CONTROLLER GAINS

Control loop	Controller gains
DC Voltage	$k_{pe} = 0.25$ $k_{ie} = 25$
DC Power	$k_{pp} = 0$ $k_{ip} = 0.5$
Current limit	$k_{pi} = 0.2$ $k_{ii} = 2$

V. Simulation Results

The "voltage wild" control scheme has been tested in simulation environment. Fig. 11 shows the results demonstrating the proposed control scheme achieving the four functionalities highlighted earlier. The operating points were selected such that each of the outer loop controllers have a distinct working region. They were picked to proof the concept of the control scheme and to not test the performance of the EPS (which will be subject for future publications).

The initial operating condition is simulated at 3100rpm, m_{lim} = 1, P_{dc}^* = 0W and the i_{smax} = 4A. P_{dc}^* is set to be lower than the actual P_{dc} so that W_e has priority on the outer loop control, unless the current limit is reached. At t = 0.3s, a step increase of P_{dc}^* = 450W is applied and reduced back at t = 1.3s. During this period, it can be observed in the figures that W_p is selected by the minimum function as i_{q3}^* is larger than i_{q1}^* in the negative direction and P_{dc} is controlled to 450W. The control action causes E_{dc} to increase in order to satisfy the power demand.

Then, the speed is increased from 3100rpm to 3200rpm at t = 1.7s and is reduced back again at t = 3s. As the speed increases, more i_d is required for flux weakening in order to maintain m = 1. This causes i_s to increase as well and eventually reaches the current limit i_{smax} = 4A. The initial overshoot of i_s is due to the nature of the open loop plant that contain double RHP zeroes. In addition to the slow time constant, the overshoot can be contained but can be difficult to be eliminated. However, some level of current overshoot are allowed in this control scheme and throughout the operation, m has been kept at 1 using the dynamic limiter.

From a general observation, it can be seen that there are different transient dynamics when the outer loop transitioning in and out of different controllers. This is due to the transient between the outer loop controllers. The bandwidths of both W_p and W_{is} are slower than W_e due to the gain limits as discussed in Section IV. As a result, transitions into W_p and W_{is} are slower in comparison to transitions into W_e. The back-tracing gain within the controller does not have significant influence during the transition due to the slower bandwidths of W_p and W_{is}.

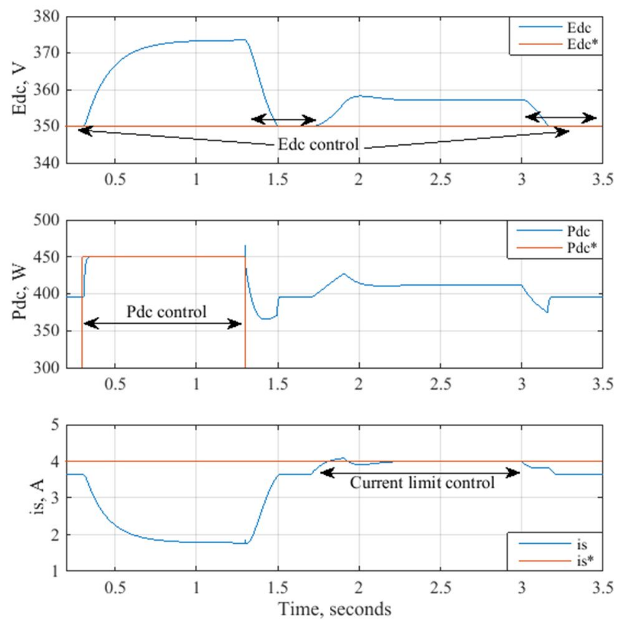

Fig. 11. Simulation results with demonstrated P_{dc} control (0.3s < t < 1.3s), i_s control (1.7s < t < 3s), and E_{dc} control.

VI. Experimental Results

An experimental rig has been used to verify the findings in this paper. The PMM (Emerson, 115UMC300CACAA) is connected to a two-level IGBT power switch AFE converter built in-house and the control platform is a DSP (Texas Instrument, TMS320C6713 DSP Starter Kit) and FPGA board. The PMM is driven by a dc brushed machine (TT Electric, LAK 2100-A) using a commercial four-quadrant dc drive (Sprint Electric, PLX 10) that acts as an active load. The power rating of the rig is much smaller in comparison to the high power demand of eWIPS as the tests aim to validate the applicability of the "voltage wild" control scheme. The operating points used are similar to the ones used in the simulation analysis.

Fig. 12 shows the results transition from constant E_{dc} control to P_{dc} control. This can be done with a change of P_{dc}^* as shown at $t \approx$ 0.9s. P_{dc} can be seen being controlled to 450W as indicated by P_{dc}^*. E_{dc} increases to satisfy the power demand that can be observed in i_q. Meanwhile, i_d adapts accordingly to maintain m = 1 during operation. The transition between the controllers can be identified when i_q^* initially following i_{q1}^* changes to i_{q3}^*.

The transition of P_{dc} back to E_{dc} control can be seen in Fig. 13. P_{dc}^* is reduced to 0W which is less than the power supplied at 350V and i_q is reduced. This triggers the constant E_{dc} controller output (i_{q1}^*) to be the priority once again as it is the smallest among the three reference signals. The different transient response is observed at about $t \approx$ 0.65s compared to when P_{dc} is operational (from Fig. 12). This is due to i_q^* being dictated by the E_{dc} controller output once P_{dc}^* was changed. Some steady state error are present when the controller is in P_{dc} control. This can be explained due to the amount of power consumed by the resistor. The resistance value can change with respect to operating temperature which affects the amount of power drawn. This error is handled by the integrator term of the controller which ensures that the correct amount of power is supplied to the load.

Fig. 14 and Fig. 15 show the results for when the outer loop control transitions between E_{dc} and current limit controllers. The operating condition was initially at 3100rpm which allows for i_s to be very close to i_s^* = 4A. The speed is then increased to 3200rpm at $t \approx$ 1s in order to increase i_s demand. i_s is perceived to be limited to i_s^* and there is a slight increase in E_{dc} to compensate for the limited current. The transition is highlighted when i_q^* changes between i_{q3}^* (P_{dc} control) and i_{q2}^* (current limit control). The different transient dynamics between the outer loop controllers can also be observed, similar to the simulation results in Fig. 11.

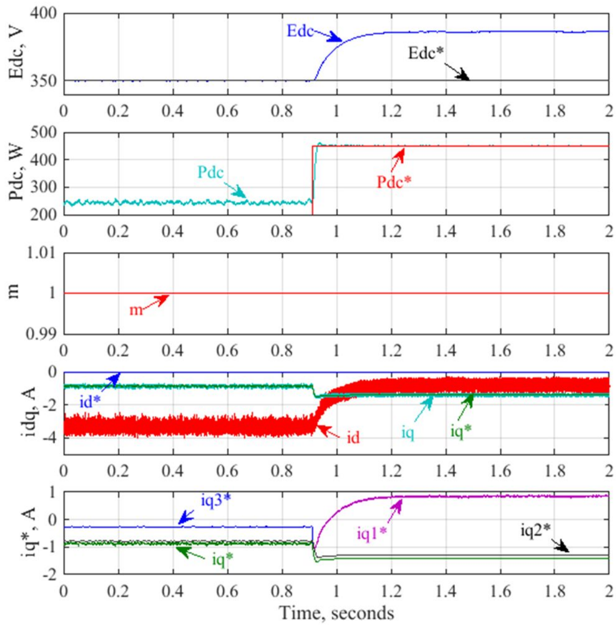

Fig. 12. P_{dc}^{*} from 0W to 450W at $t \approx 0.9$s.

It is to be noted that throughout the control operation, m has been kept within the limit of 1 via flux weakening. In general, the experimental results demonstrate the functionalities of the proposed control scheme.

VII. Conclusion

The new 'voltage-wild' concept has been investigated for an aircraft EPS with eWIPS load. Its novel control scheme was proposed with the strategy to cover the concepts four main functionalities; E_{dc}, m, P_{dc}, and current limit control. The small signal control plants for the controllers have been derived for controller design process. Non-minimum phase characteristics was inherent for both P_{dc} and current limit

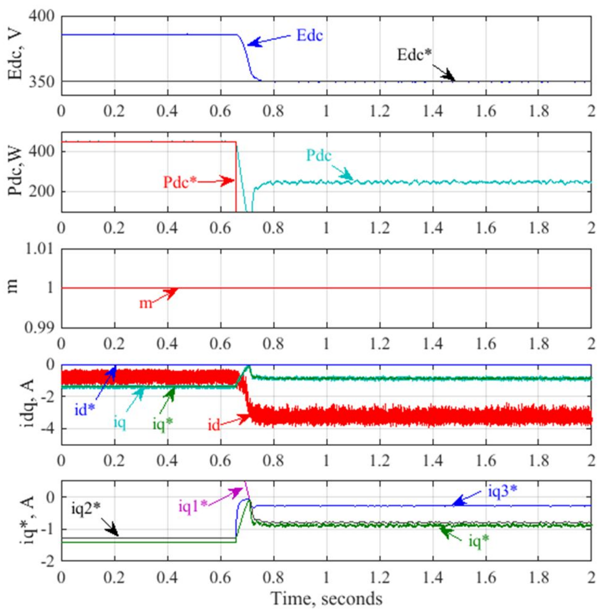

Fig. 14. P_{dc}^{*} from 450W to 0W at $t \approx 0.65$s.

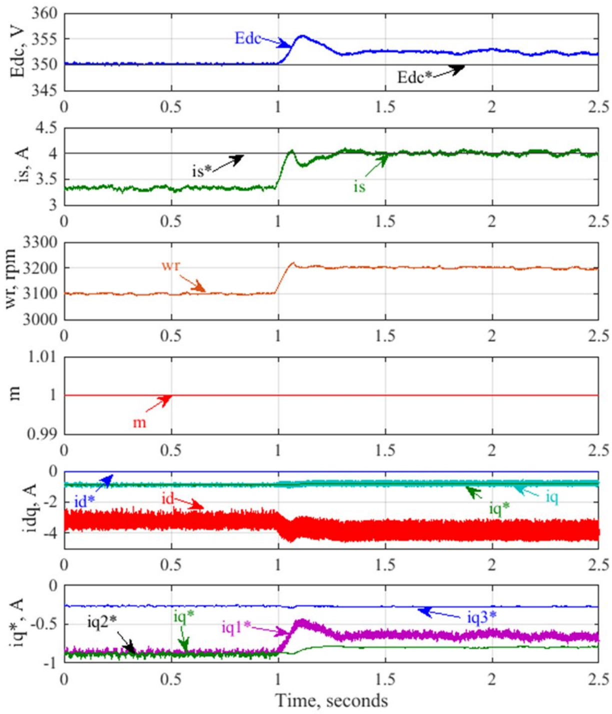

Fig. 15. Speed change from 3100rpm to 3200rpm at $t \approx 1$s.

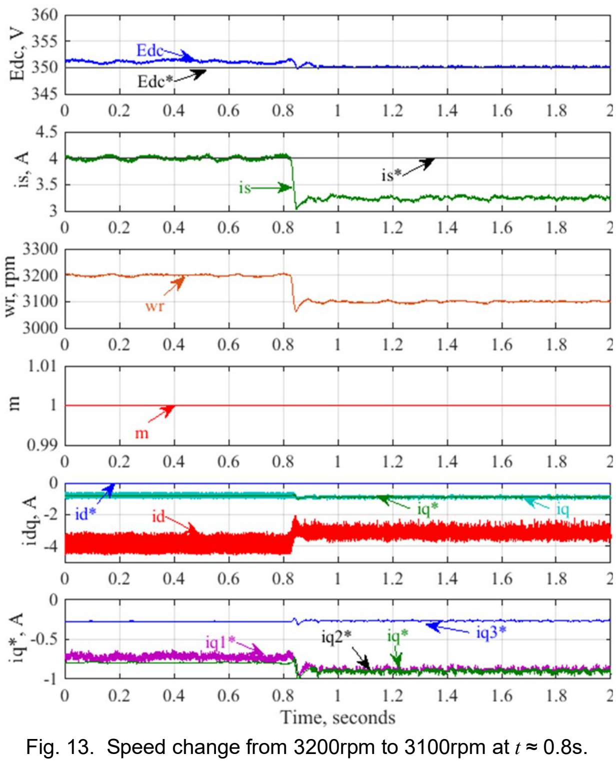

Fig. 13. Speed change from 3200rpm to 3100rpm at $t \approx 0.8$s.

plants, which meant limited gain stability for the associated controllers. Simulations have been performed in order to demonstrate the control operation for each of the functionalities. Experimental testing has also been done to proof the variable voltage concept on a mock-up EPS. For future studies, the EPS shall be expanded to cover multiple buses to emulate a larger aircraft EPS. This allows investigation of control stability at different flight conditions and the supervisor control strategy of the EPS.

REFERENCES

[1] B. Sarlioglu and C. T. Morris, "More Electric Aircraft: Review, Challenges, and Opportunities for Commercial Transport Aircraft," *IEEE Trans. Transport. Elec.*, vol. 1, pp. 54-64, 2015.
[2] P. Wheeler and S. Bozhko, "The More Electric Aircraft: Technology and challenges," *Electrification Magazine, IEEE,* vol. 2, pp. 6-12, 2014.
[3] S. Bozhko, T. Yang, J. L. Peuvedic, P. Arumugam, M. Degano, A. L. Rocca, Z. Xu, M. Rashed, W. Fernando, C. I. Hill, C. Eastwick, S. Pickering, C. Gerada, and P. Wheeler, "Development of Aircraft Electric Starter-Generator System Based-On Active Rectification Technology," *IEEE Transactions on Transportation Electrification,* pp. 1-1, 2018.
[4] I. Moir and A. Seabridge, *Aircraft Systems: Mechanical, Electrical and Avionics Subsystems Integration*: Wiley, 2008.
[5] Z. Goraj, "An Overview of the De-Icing and Anti-Icing Technologies with Prospects for the Future," presented at the 24th Congress of International Council of the Aeronautical Sciences ICAS, Yokohama, Japan, 2004.
[6] F. Abdesselam, L. Boissy, A. Castellazzi, T. Wijekoon, P. Wheeler, and M. Johnson, "Preliminary study for the integrated design of an electro-mechanical wing de-icing system," in *2010 6th International Conference on Integrated Power Electronics Systems*, 2010, pp. 1-6.
[7] X. Roboam, B. Sareni, and A. D. Andrade, "More Electricity in the Air: Toward Optimized Electrical Networks Embedded in More-Electrical Aircraft," *Industrial Electronics Magazine, IEEE,* vol. 6, pp. 6-17, 2012.
[8] B. H. Nya, J. Brombach, and D. Schulz, "Benefits of higher voltage levels in aircraft electrical power systems," in *Electrical Systems for Aircraft, Railway and Ship Propulsion (ESARS), 2012*, 2012, pp. 1-5.
[9] N. Devillers, D. Bienaime, M. C. Pera, and F. Gustin, "Study and Assessment by Simulation of Aircraft Full DC Electrical Power System and Energy Management: Special Session on EMR and Other Graphic Description," in *2015 IEEE Vehicle Power and Propulsion Conference (VPPC)*, 2015, pp. 1-6.
[10] U. Electronics. (2011). *Ice Protection Systems*. Available: https://www.ultra-pcs.com/app/uploads/2017/06/Brochure-Ice-Protection-Systems.pdf. Accessed: 13/3/2018
[11] S. Bozhko, M. Rashed, C. I. Hill, S. S. Yeoh, and T. Yang, "Flux-Weakening Control of Electric Starter-Generator Based on Permanent-Magnet Machine," *IEEE Transactions on Transportation Electrification,* vol. 3, pp. 864-877, 2017.
[12] S. S. Yeoh, F. Gao, S. Bozhko, and G. Asher, "Control design for PMM-based starter generator system for More Electric Aircraft," in *Power Electronics and Applications (EPE'14-ECCE Europe)*, 2014, pp. 1-10.
[13] D. Stojan, D. Drevensek, Z. Plantic, B. Grcar, and G. Stumberger, "Novel field weakening control scheme for permanent magnet synchronous machines based on voltage angle control," *Industry Applications, IEEE Transactions on,* vol. PP, pp. 1-1, 2012.
[14] H. Lee, J. Kim, J. Hong, and K. Nam, "Torque control for IPMSM in the high speed range based on voltage angle," in *2014 IEEE Applied Power Electronics Conference and Exposition - APEC 2014*, 2014, pp. 2500-2505.
[15] F. Gao, S. Bozhko, A. Costabeber, G. Asher, and P. Wheeler, "Control Design and Voltage Stability Analysis of a Droop-Controlled Electrical Power System for More Electric Aircraft," *IEEE Transactions on Industrial Electronics,* vol. 64, pp. 9271-9281, 2017.
[16] G. Fei, S. Bozhko, Y. Seang, G. Asher, and P. Wheeler, "Stability of multi-source droop-controlled Electrical Power System for more-electric aircraft," in *Intelligent Energy and Power Systems (IEPS), 2014 IEEE International Conference on*, 2014, pp. 122-126.
[17] P. C. Krause, O. Wasynczuk, S. D. Sudhoff, and I. P. E. Society, *Analysis of electric machinery and drive systems*: IEEE Press, 2002.
[18] A. Eid, H. El-Kishky, M. Abdel-Salam, and T. El-Mohandes, "Modeling and characterization of an aircraft electric power system with a fuel cell-equipped APU connected at HVDC bus," in *Power Modulator and High Voltage Conference (IPMHVC), 2010 IEEE International*, 2010, pp. 639-642.
[19] M. Yin, S. Bozhko, and S. S. Yeoh, "Control Design for PMM-Based Generator Fed by Active Front-End Rectifier in More-Electric Aircraft," *SAE Int. J. Aerosp.,* vol. 9, pp. 23-29, 2016.
[20] D. M. Miao, Y. Mollet, J. Gyselinck, and J. X. Shen, "DC Voltage Control of a Wide-Speed-Range Permanent-Magnet Synchronous Generator System for More Electric Aircraft Applications," in *2016 IEEE Vehicle Power and Propulsion Conference (VPPC)*, 2016, pp. 1-6.
[21] A. Yazdani and R. Iravani, *Voltage-Sourced Converters in Power Systems*: John Wiley & Sons, Inc., 2010.
[22] H. B. Enalou and E. A. Soreshjani, "A Detailed Governor-Turbine Model for Heavy-Duty Gas Turbines With a Careful Scrutiny of Governor Features," *IEEE Transactions on Power Systems,* vol. 30, pp. 1435-1441, 2015.
[23] S. Bozhko, S. S. Yeoh, F. Gao, and C. Hill, "Aircraft starter-generator system based on permanent-magnet machine fed by active front-end rectifier," in *Industrial Electronics Society (IECON)*, 2014, pp. 2958-2964.

APPENDIX I: EPS PARAMETERS

Parameter	Variable	Value
Machine rated power	P_{rated}	2540W
Machine rated speed	ω_r	3400rpm
Machine rated current	i_{rated}	5A
Stator resistance	R_s	1.2Ω
d-axis stator inductance	L_d	6.17mH
q-axis stator inductance	L_q	8.38mH
Magnet flux	ψ_m	0.23Wb
Pole pairs	p	3
DC bus capacitance	C	1mF
Sampling frequency	f_s	12500Hz
i_d PI controller gains	k_{pid}, k_{iid}	12.28, 8428
i_q PI controller gains	k_{piq}, k_{iiq}	15.99, 10724

APPENDIX II: TRANSFER FUNCTION COEFFICIENTS

$$n_1 = L_d L_q \left(i_{qo} m_{do} - i_{do} m_{qo}\right), n_2 = R_s i_{qo} m_{do}\left(L_d + L_q\right) - R_s i_{do} m_{qo}\left(L_d + L_q\right) - L_q m_{qo} v_{do} + L_d m_{do} v_{qo}$$

$$n_3 = -R_s m_{qo} v_{do} + R_s m_{do} v_{qo} + L_q m_{do} v_{do} \omega_{eo} + L_d m_{qo} v_{qo} \omega_{eo} + i_{qo} m_{do}\left(R_s^2 + L_d L_q \omega_{eo}^2\right) - i_{do} m_{qo}\left(R_s^2 + L_d L_q \omega_{eo}^2\right)$$

$$n_4 = 2CE_{dco}^2 R_w \left(i_{qo} L_d m_{do} - i_{do} L_q m_{qo}\right), n_5 = 3E_{dco} i_{do} i_{qo} k_s R_w \left(L_d - L_q\right)\left(m_{do}^2 + m_{qo}^2\right) + 3R_w\left(-i_{qo} L_d m_{do} + i_{do} L_q m_{qo}\right)\left(i_{do} v_{do} + i_{qo} v_{qo}\right)$$

$$+2E_{dco}^2\left(-i_{do}\left(R_s C m_{qo} R_w + L_q\left(m_{qo} - C m_{do} R_w \omega_{eo}\right)\right) + i_{qo}\left(R_s C m_{do} R_w + L_d\left(m_{do} + C m_{qo} R_w \omega_{eo}\right)\right)\right)$$

$$n_6 = 2E_{dco}^2\left(i_{do}\left(-R_s m_{qo} + L_q m_{do} \omega_{eo}\right) + i_{qo}\left(R_s m_{do} + L_d m_{qo} \omega_{eo}\right)\right) + 3E_{dco} k_s R_w \left(m_{do}^2 + m_{qo}^2\right)\left(i_{qo} v_{do} + i_{qo}^2 L_d \omega_{eo} + i_{do}\left(-v_{qo} + i_{do} L_q \omega_{eo}\right)\right)$$

$$+3R_w\left(i_{do} v_{do} + i_{qo} v_{qo}\right)\left(i_{do}\left(R_s m_{qo} - L_q m_{do} \omega_{eo}\right) - i_{qo}\left(R_s m_{do} + L_d m_{qo} \omega_{eo}\right)\right)$$

$$d_1 = 2CE_{dco}{}^2 L_d R_w m_{do}, d_2 = 3E_{dco} i_{do} k_s L_d R_w \left(m_{do}^2 + m_{qo}^2\right) - 3L_d m_{do} R_w \left(i_{do} v_{do} + i_{qo} v_{qo}\right) + 2E_{dco}^2\left(R_s C m_{do} R_w + L_d\left(m_{do} + C m_{qo} R_w \omega_{eo}\right)\right)$$

$$d_3 = 3E_{dco} k_s R_w \left(m_{do}^2 + m_{qo}^2\right)\left(R_s i_{do} + v_{do} + i_{qo} L_d \omega_{eo}\right) + 2E_{dco}^2\left(R_s m_{do} + L_d m_{qo} \omega_{eo}\right) - 3R_w\left(i_{do} v_{do} + i_{qo} v_{qo}\right)\left(R_s m_{do} + L_d m_{qo} \omega_{eo}\right)$$

$$d_4 = 2CE_{dco}{}^2 L_d R_w m_{do}, d_5 = 3E_{dco} i_{do} k_s L_d R_w \left(m_{do}^2 + m_{qo}^2\right) - 3L_d m_{do} R_w \left(i_{do} v_{do} + i_{qo} v_{qo}\right) + 2E_{dco}^2\left(R_s C m_{do} R_w + L_d\left(m_{do} + C m_{qo} R_w \omega_{eo}\right)\right)$$

$$d_6 = 3E_{dco} k_s R_w \left(m_{do}^2 + m_{qo}^2\right)\left(R_s i_{do} + v_{do} + i_{qo} L_d \omega_{eo}\right) + 2E_{dco}^2\left(R_s m_{do} + L_d m_{qo} \omega_{eo}\right) - 3R_w\left(i_{do} v_{do} + i_{qo} v_{qo}\right)\left(R_s m_{do} + L_d m_{qo} \omega_{eo}\right)$$

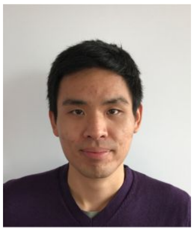

Seang Shen Yeoh received his MSc degree in power electronics (Distinction) and Ph.D degree in electrical engineering from the University of Nottingham, United Kingdom, in 2011 and 2016 respectively. Since then, he has been a research fellow in the same university under the Power Electronics, Machines, and Controls Research Group. His current research interests are in the area of aircraft application, namely modelling and stability studies of complex power systems, and new control strategies for high speed drive systems.

Mike Sanders went to Coventry (Lanchester) Polytechnic (now Coventry University) where he received his degree in Combined Engineering. He started his professional career with British Aerospace in 1984 under the Airframe Electrical Systems Department. He also worked on both civil (Advanced Turbo Prop, Jetstream 41) and military programmes (Nimrod AEW3). He is currently with Meggitt (since 1995) as Systems Technology Manager responsible for Applied Research and Technology Ice Protection projects.

Mohamed Rashed (M'07) received the Ph.D. degree in electrical motor drives from the University of Aberdeen, Aberdeen, U.K., in 2002. He was a Post-Doctoral Research Fellow with the Department of Engineering, University of Aberdeen for the periods, from 2002 to 2005 and from 2007 to 2009. In 2005, he was appointed as an Assistant Professor with the Department of Electrical Engineering, Mansoura University, Mansoura, Egypt, and then on leave from 2007. In 2008, he was promoted to an Associate Professor in Mansoura University, Egypt. In 2009, he joined the Power Electronics, Machines and Control Research Group, Department of Electrical and Electronic Engineering, The University of Nottingham, Nottingham, U.K., where he is currently a Senior Research Fellow. His current research interests include the design and control of electrical motor drives and power systems for aerospace applications, power electronics for micro grids, renewable energy sources, and energy storage systems.

Serhiy Bozhko (M'1997, SM'2018) received his M.Sc. and Ph.D. degrees in electromechanical systems from the National Technical University of Ukraine, Kyiv City, Ukraine, in 1987 and 1994, respectively. Since 2000, he has been with the Power Electronics, Machines and Controls Research Group of the University of Nottingham, United Kingdom, where currently he is Professor of Aircraft Electric Power Systems and Director of the Institute for Aerospace Technology.

He is leading several EU- and industry funded projects in the area of aircraft electric power systems, including power generation, distribution and conversion, power quality, control and stability issues, power management and optimisation, as well as advanced modelling and simulations methods.